Supporting Information

Single-atom cobalt-hydroxyl modification of polymeric carbon nitride for highly enhanced photocatalytic water oxidation: ball milling increased single atom loading

Content

S1. Synthesis of samples

S1.1. Synthesis of PCN and BM-PCN

Bulk PCN was prepared via direct pyrolysis of melamine. Simply, melamine (10 g, 99%, Aladdin) was added in a crucible with a lid, calcined at 550 °C for 4 h in a muffle furnace with a ramp rate of 5 °C min^{-1}, and then cooled naturally to room temperature. Gained hard yellow solid was ground into powders for use.

For synthesis of BM-PCN, PCN (1.0 g) was transferred into a 100-mL zirconia jar containing agate balls (110 g) with diameters of 3 mm (20 g), 5 mm (23 g), 8 mm (30 g), and 10 mm (37 g). Then, four agate jars were fixed in a planetary ball mill (TECHIN TJX-450, Tianjin, China) and agitated at 1500 rpm for 6 h.

S1.2. Synthesis of BM-PCN/Co-c and PCN/Co-c

Typically, BM-PCN (0.5 g) was dispersed in $CoCl_2 \cdot 6H_2O$ (99.99%, Aladdin) solution (0.10 M, 50 mL) by sonification for 10 min. After stirring for 1 h, the solid (marked as BM-PCN/Co) was collected by filtration, washed with water (10 mL), and dried at 60 °C for 12 h. BM-PCN/Co was then calcined at 460 °C for 2 h in air with a ramp rate of 5 °C min^{-1}. After cooled to room temperature, the powders were washed with water and dried at 60 °C for 12 h to obtain BM-PCN/Co-c. To optimize Co^{2+} concentrations, the $CoCl_2$ solution with a concentration (x M) of 0.05, 0.15, or 0.20 M was also used and the product was marked as BM-PCN/Cox-c. To optimize the calcination temperature (T_c °C) of BM-PCN/Co, 440, 480, and 500 °C were also investigated and the products were marked as BM-PCN/Co-cT_c. PCN/Co-c was synthesized similarly as BM-PCN/Co-c except PCN was used as the feedstock. The product BM-PCN-c was prepared by direct calcination of BM-PCN (0.5 g) without Co^{2+} adsorption.

S1.3. Preparation of PCN/CoO$_x$

PCN/CoO$_x$ was synthesized according to reported work [1]. PCN (50 mg) was dispersed in ultrapure water (80 mL) by sonification for 5 min. Then, the $CoCl_2 \cdot 6H_2O$ solution (2 g L^{-1}, 765 μL) was added to the dispersion and stirred for 10 min, after which the suspension was illuminated by a CEL-PF300-T8E Xe lamp (200 W, Ceaulight) for 4 h. The product was obtained after filtration, washed with water, and dried at 60 °C for 12 h.

S1.4. Preparation of PCN-urea and PCN-urea/Co-c

For synthesis of PCN-urea, urea (10 g, 99%, Aladdin) was added in a crucible with a lid, calcined at 550 °C for 4 h in a muffle furnace with a ramp rate of 5 °C min^{-1}, and then cooled naturally to room temperature. The gained product was ground into powders for use.

PCN-urea/Co-c was synthesized similarly as BM-PCN/Co-c. Simply, PCN-urea (0.5 g) was dispersed in $CoCl_2$ solution (0.10 M, 50 mL) by sonification for 10 min. After stirring for 1 h, the solid was collected by filtration, washed with water (10 mL), dried at 60 °C for 12 h, and then calcined at 460 °C for 2 h in air with a ramp rate of 5 °C min^{-1}. After cooled to room temperature, the solid powders were washed with water and dried at 60 °C for 12 h to obtain PCN-urea/Co-c. To optimize Co^{2+} concentrations, the $CoCl_2$ solution with a concentration (x M) of 0.05 or 0.15 M was also used and the product was marked as PCN-urea/Cox-c.

S1.5. Preparation of BM-PCN-c/Co(OH)$_2$

For synthesis of BM-PCN-c/Co(OH)$_2$ [2], BM-PCN-c (50 mg) was dispersed in ultrapure water (10 mL) by sonification for 10 min and the $Co(NO_3)_2 \cdot 6H_2O$ (99.99%, Aladdin) solution (2 g L^{-1}, 925 μL) was added to the dispersion. After stirring for 20 min, the concentrated ammonia solution (28%, 1 mL) was slowly dropped to the dispersion under stirring and then the dispersion continued to be stirred for 30 min. The green precipitate was collected by filtration, washed with water, and dried at 60 °C for 12 h to obtain the product.

S2. Characterizations

X-ray diffraction (XRD) tests were conducted on a Rigaku SmartLab 9KW in-situ X-ray diffractometer (Japan) with Cu-Kα radiation. A Bruker ALPHA spectrophotometer (Germany) was used for Fourier-transform infrared (FT-IR) spectroscopy analysis. Morphologies of samples were observed by transmission electron microscopy (TEM, Jeol JEM-1011, Japan), field emission-scanning electron microscopy (SEM, Hitachi SU8010, Japan), atomic force microscopy (AFM, Digital Instruments Nanoscope IIIa), and aberration-corrected high-angle annular dark-field scanning transmission electron microscopy (HAADF-STEM, FEI Themis Z, USA). Energy dispersive spectroscopy (EDS) was performed on the SEM equipment. Elemental analysis on an Elementar Vario EL III apparatus (Germany) and inductively coupled plasma-mass spectrometry (ICP-MS) (NexION^{TM} 350X, PerkinElmer, USA) were performed to determine compositions of samples. Zeta potentials of particles were measured on a Zetasizer Nano ZS apparatus (Malvern Instruments, UK). X-ray photoelectron spectroscopy (XPS) was performed on an ESCALAB 250XI spectrometer (Thermo Fisher, USA). The C 1s peak at 284.6 eV was used to calibrate peak positions. Nitrogen sorption isotherms were tested on a Quadrasorb EVO analyzer (Quantachrome Instruments, USA), with degassing temperature and time of 100 °C and 6 h, respectively. The solid-state ^{13}C magic-angle spinning (MAS) nuclear magnetic resonance (NMR) spectroscopy was carried out on an Agilent 600MHz spectrometer (USA). UV-vis diffuse reflectance spectroscopy (DRS) was performed on a Hitachi U4100 UV Spectrometer (Japan). Electron paramagnetic resonance (EPR) spectroscopy was conducted on a Bruker A300-10/12 spectrometer (Germany) at room temperature (microwave frequency, 9.85 GHz; center field, 3510 G; sweep width, 100 G; modulation frequency, 100 kHz; and modulation amplitude, 1.00 G), in the dark or upon successive irradiation with a 300-W Xe lamp (CEL-HXF300, Ceaulight, China) equipped with a cutoff filter ($\lambda \geq$ 420 nm) as the visible light source. Photoluminescence (PL) spectroscopy was performed on a Horiba FluoroMax-4 spectrophotometer (Japan) at room temperature, with the excitation

wavelength of 400 nm and excitation and emission slit width of 1 nm. X-ray absorption spectroscopy (XAS) including X-ray absorption near-edge structure spectroscopy (XANES) and extended X-ray absorption fine structure (EXAFS) analysis was performed for the Co K-edge measurement of samples at the Beamline of TLS07A1 in National Synchrotron Radiation Research Center (Taiwan, China). Co foil, Co porphyrin ([5,10,15,20-tetrakis(4-methoxyphenyl)porphyrinato]cobalt(II)), CoO, Co_2O_3, and Co_3O_4 were used as reference samples.

S3. Time-resolved fluorescence spectroscopy

Time-resolved fluorescence spectroscopy was carried out on an Edinburg FLS 920 spectrometer (UK) with excitation and monitoring wavelengths of 405 and 465 nm, respectively. The decay curve was fitted to a triple-exponential model (till χ^2 close to 1),

$\qquad I = B_1 \cdot \exp(-t/\tau_1) + B_2 \cdot \exp(-t/\tau_2) + B_3 \cdot \exp(-t/\tau_3)$ $\qquad\qquad\qquad$ (1)

where I, $\tau_1–\tau_3$, and $B_1–B_3$ are the intensity, the fluorescence lifetimes, and the amplitudes of components, respectively. [3] The average fluorescence lifetime (τ_m) was calculated via the equation,

$\qquad \tau_m = (R_1 \cdot \tau_1^2 + R_2 \cdot \tau_2^2 + R_3 \cdot \tau_3^2)/(R_1 \cdot \tau_1 + R_2 \cdot \tau_2 + R_3 \cdot \tau_3)$ $\qquad\qquad$ (2)

where $R_1–R_3$ are the percentages of $\tau_1–\tau_3$, respectively. [4]

S4. Photoelectrochemical tests

Photoelectrochemical measurement was performed on a CHI660E electrochemical workstation (Chenhua, China) equipped with a three-electrode system (a working electrode, a counter electrode (Pt sheet), and an Ag/AgCl reference electrode). To prepare the working electrode, the mixture of the sample (20 mg) and ethylene glycol (400 μL) was ground for 1 min in a mortar and then taken to coat the (1 cm × 1 cm) area on clean ITO glass by the doctor-blade method. The electrode was dried at 60 °C for 12 h and calcined at 200 °C for 2 h in the nitrogen atmosphere. Potentials (vs. Ag/AgCl) were adjusted to those (vs. SHE) via the equation,

$\qquad E_{SHE}$ (V) $= E_{Ag/AgCl}$ (V) $+ 0.197$ V $\qquad\qquad\qquad\qquad\qquad\qquad$ (3).

Photocurrent density was tested at a bias voltage of 0.6 V in 0.2 M Na_2SO_4 solution. The visible light source was a 300-W Xe lamp (CEL-HXF300, Ceaulight) equipped with a cutoff filter ($\lambda \geq 420$ nm). Mott-Schottky and Electrochemical impedance spectroscopy (EIS) tests were carried out in the 0.1 M KCl solution including 2.5 mM $K_3Fe(CN)_6$ and 2.5 mM $K_4Fe(CN)_6$, with frequencies set as 1.0 kHz. Electrochemical impedance spectroscopy (EIS) data were taken in a frequency range of $0.01–10^4$ Hz with an AC voltage of 5 mV and a bias voltage of 0.2 V.

S5. Theoretical calculations

Density functional theory (DFT) calculations were performed using the Vienna ab initio simulation package. Projector augmented wave (PAW) potentials [5-7] and Perdew-Burke-Ernzerhof (PBE) functional within the generalized gradient approximation (GGA) [8] were used in the calculation. The vacuum space along the z-direction was set to be 15 Å. Cutoff energy was set to be 500 eV, and the k-point sampling grid is 3×4×1. Convergence tolerances of energy and force were set as 1.0×10^{-4} eV atom^{-1} and 10^{-2} eV Å^{-1}, respectively. Moreover, the DFT-D3 method was used to describe van der Waals interaction in this work [9]. The lattice constant of monolayer PCN, namely C_2N_3H, was calculated to be $a = 16.82$ Å and $b = 12.81$ Å, close to reported results [10].

$\qquad$ Formation energy (E) of Co doped PCN can be estimated as

$\qquad\qquad E = E$(doped) $- E$(PCN) $- \mu_{Co} + m\mu_H - n\mu_O$ $\qquad\qquad\qquad\qquad$ (4).

Here, E(doped) is the total energy of Co doped PCN. E(PCN) is the total energy of PCN. The μ_{Co} is the chemical potential of one Co atom in bulk Co. The μ_H is the chemical potential of one H atom in H_2. The μ_O is the chemical potential of one O atom in O_2. The m in Co-N_3 and Co-N_4 is 2. The m and n in Co-N_4OH are 0 and 1, respectively.

S6. Photocatalytic water oxidation

All of photocatalytic O_2 evolution tests were conducted on a CEL-SPH2N-D photoactivity-evaluation system (Ceaulight, China). First, the photocatalyst (50 mg) and La_2O_3 (0.2 g) were dispersed in $AgNO_3$ aqueous solution (0.1 M, 80 mL) by sonification for 5 min. Then, the dispersion was evacuated under stirring and the O_2 evolution was started under illumination of a CEL-PF300-T8E Xe lamp (200 W and ~730 mW cm^{-2} measured by a CEL-NP2000 optical power meter, Ceaulight) or the Xe lamp equipped with a cutoff filter ($\lambda \geq 420$ nm, ~540 mW cm^{-2}) and the produced O_2 was tested via an on-line gas chromatograph (GC-7920, Ceaulight) with a thermal conductivity detector (TCD), using ultrapure Ar as the carrier gas. To determine apparent quantum yields (AQYs) of the photocatalyst, O_2 evolution rates were measured under irradiation of monochromatic light which was derived by substituting a series of Thorlabs band-pass filters (400–500 nm, USA) for above ≥420-nm cutoff filter. The AQY can be calculated by the equation,

$\qquad$ AQY $= 4R_O/(E_i \cdot A/E_p) \times 100\%$ $\qquad\qquad\qquad\qquad\qquad\qquad$ (5)

where R_O, E_p, A, and E_i are the O_2 evolution rate (mol s^{-1}), the photon energy (J mol^{-1}), the irradiation area (cm^2), and the irradiation intensity (W cm^{-2}, minus the transmission light intensity), respectively.

$\qquad$ For the cyclic OER experiment on BM-PCN/Co-c, KIO_4 (0.01 M) was substituted for $AgNO_3$ as the sacrificial agent. After one run, the system was evacuated and re-started by illumination of the Xe lamp. After completing the experiment, the solid was collected by filtration, washed with water and dried at 60 °C for 12 h.
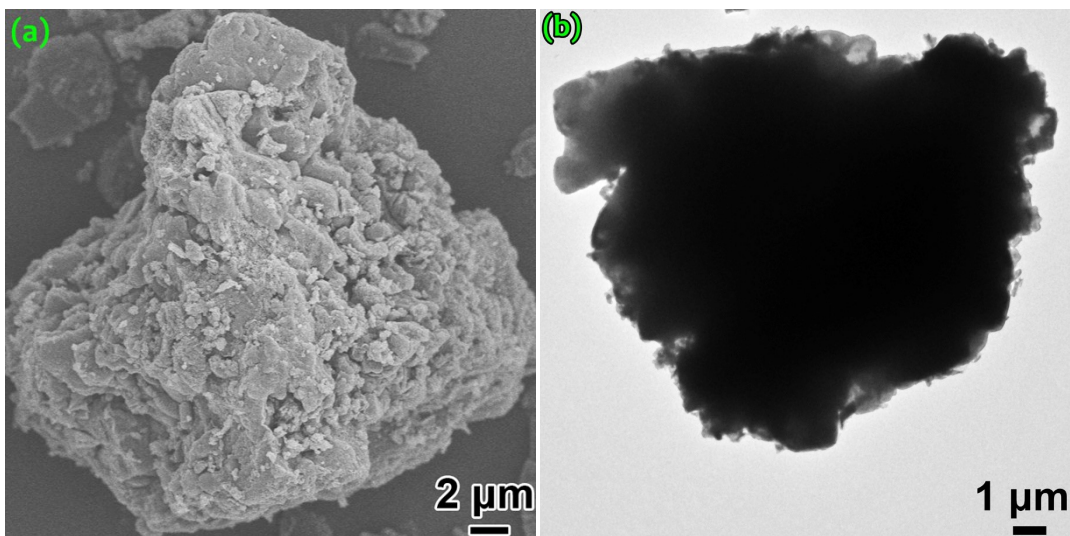
Fig. S1. (a) SEM and (b) TEM images of PCN.
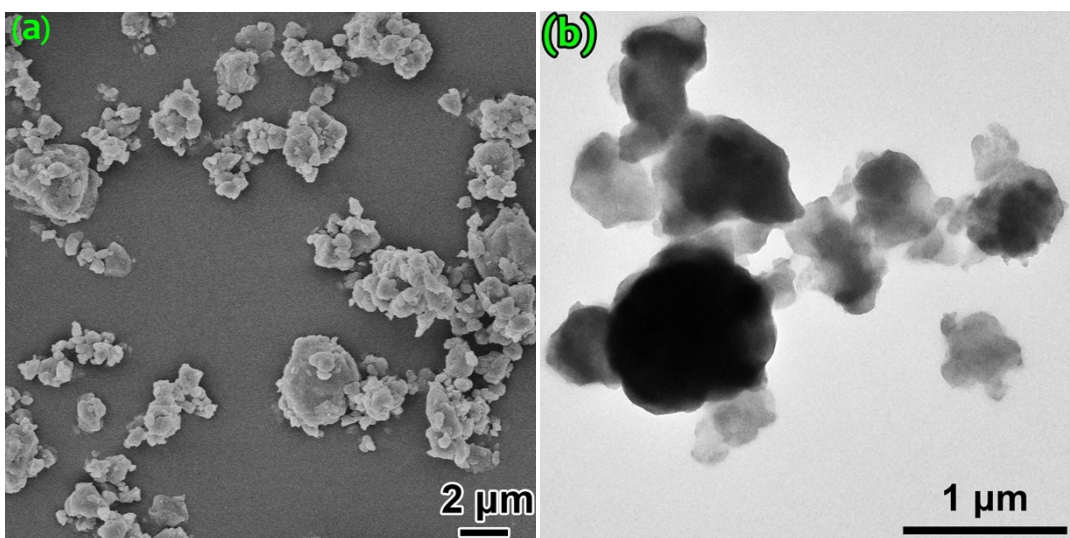
Fig. S2. (a) SEM and (b) TEM images of BM-PCN.
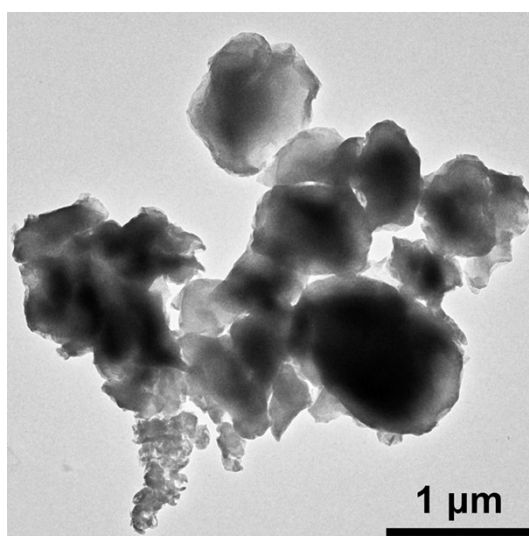
Fig. S3. The TEM image of BM-PCN/Co-c.
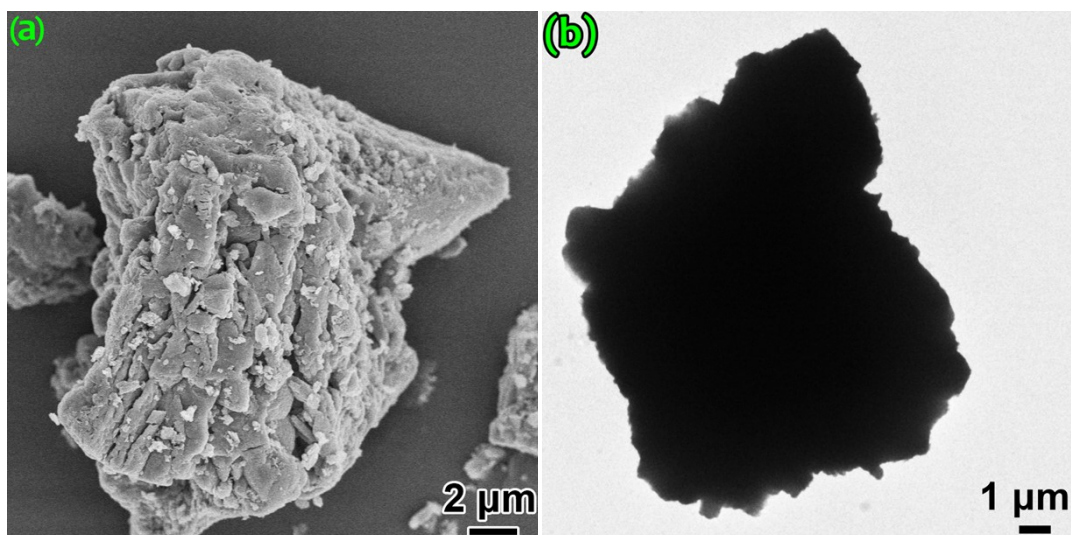
Fig. S4. (a) SEM and (b) TEM images of PCN/Co-c.
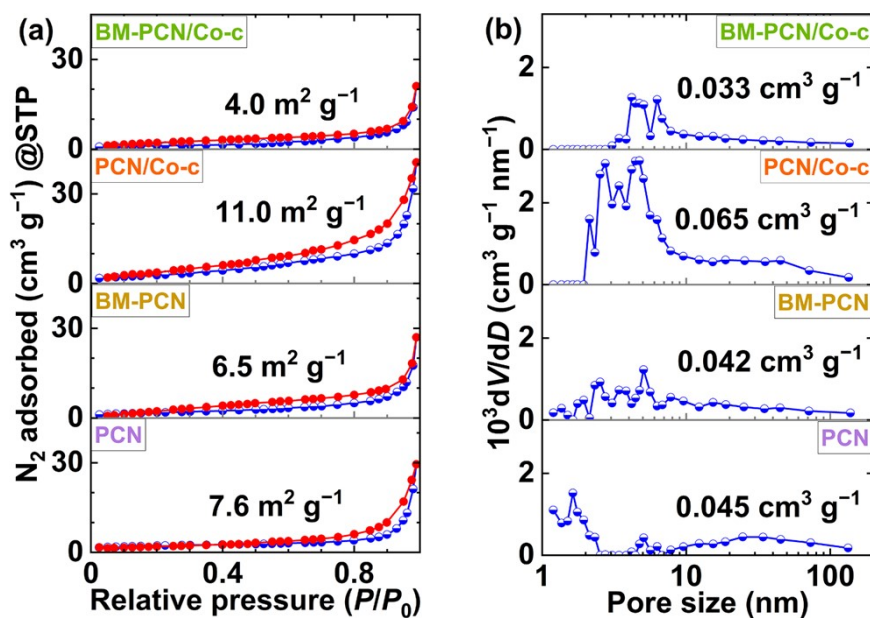
Fig. S5. (a) Nitrogen sorption isotherms of samples and (b) pore-size distribution curves gained by calculating adsorption branches of corresponding isotherms by a BJH method. Numbers in (a) and (b) are specific surface area and pore volume, respectively.
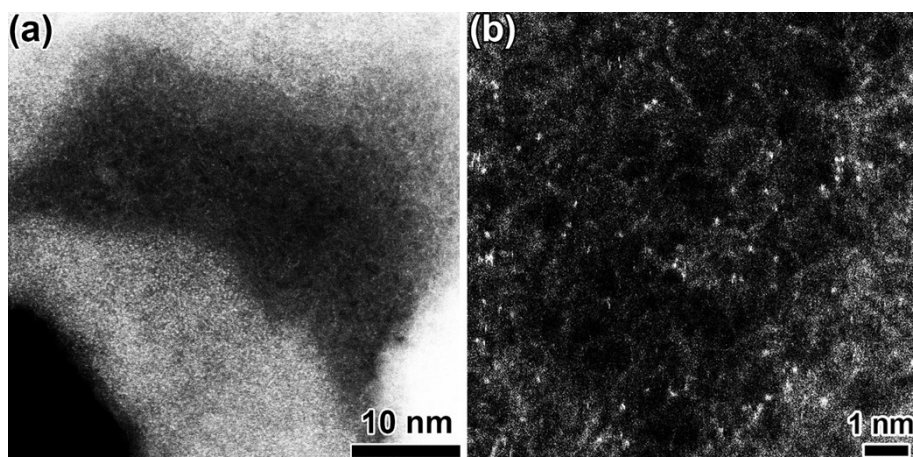
Fig. S6. The HAADF-STEM images of BM-PCN/Co-c.
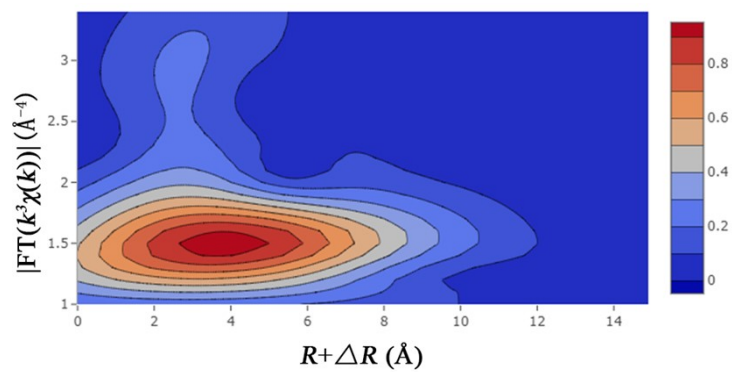
Fig. S7. The Wavelet transform (WT) contour plot of BM-PCN/Co-c.
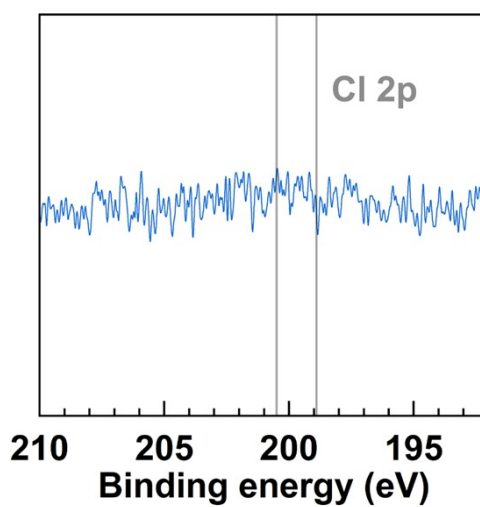
Fig. S8. The Cl 2p core-level XPS spectrum of BM-PCN/Co-c.
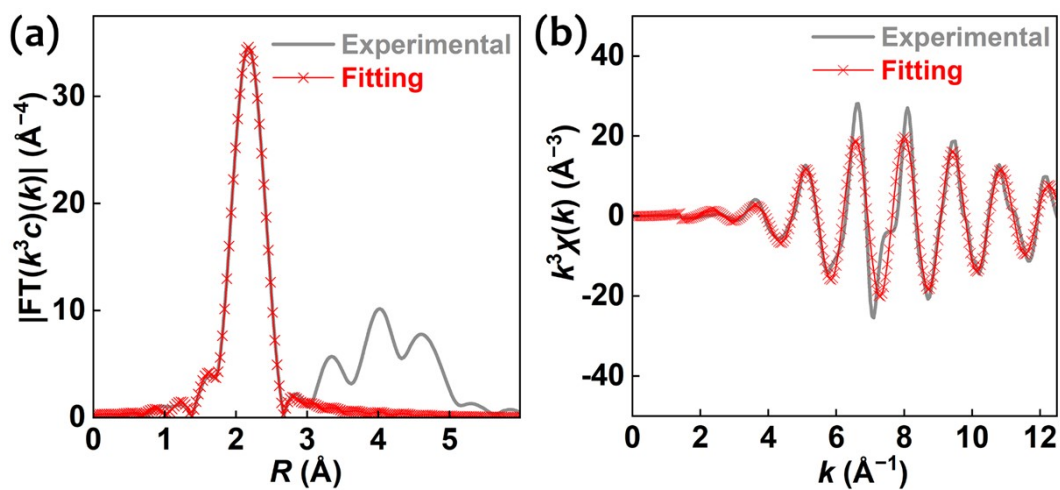
Fig. S9. Fourier-transformed magnitude of Co K-edge EXAFS spectra in (a) R space and (b) k space for Co foil. Measured and calculated spectra are well matched. The best-fitting parameters are shown in Table S1.
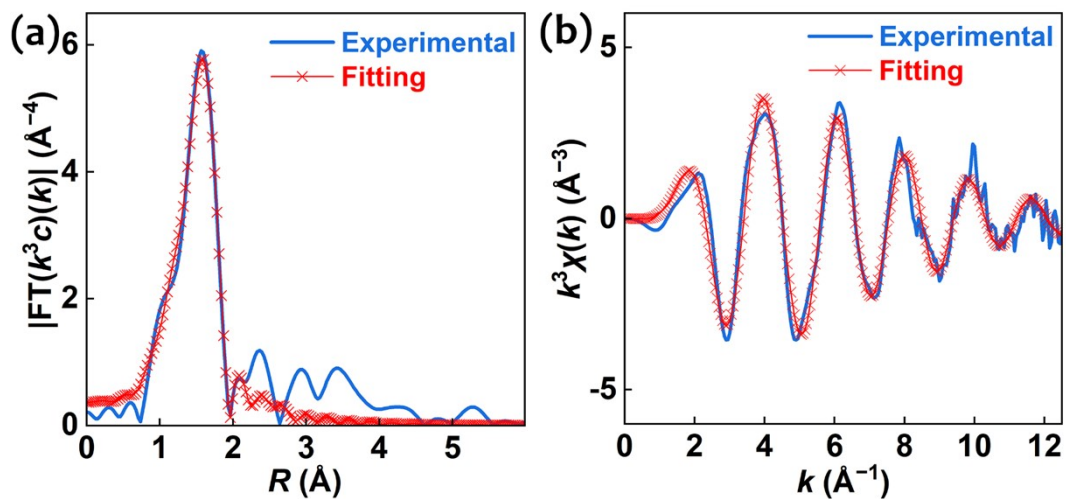
Fig. S10. Fourier-transformed magnitude of Co K-edge EXAFS spectra in (a) *R* space and (b) *k* space for BM-PCN/Co-c. Measured and simple single-shell fitting spectra are basically matched. The best-fitting parameters are shown in Table S1.
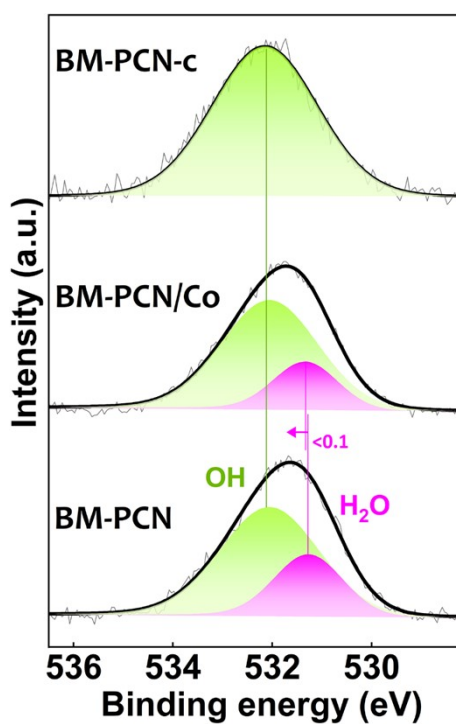
Fig. S11. The O 1s core-level XPS spectra of samples.
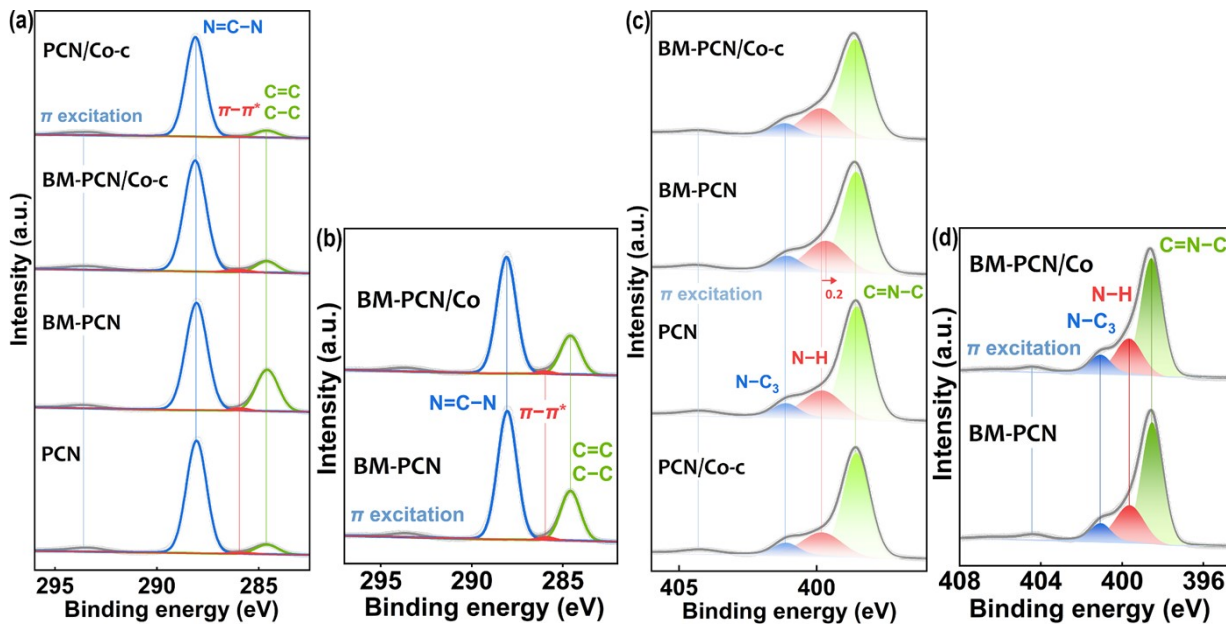
Fig. S12. (a and b) C 1s and (c and d) N 1s core-level XPS spectra of samples.

In C 1s core-level XPS spectra of the samples, PCN exhibits typical four peaks at binding energy of 284.6, 286.0, 288.1, and 293.6 eV (Fig. S12a), ascribed to adventitious carbon, π-π^* of carbon cycles [11], N=C−N, and π excitation of heptazine cycles [12, 13], respectively. The BM-PCN, BM-PCN/Co-c, PCN/Co-c, and BM-PCN/Co (Fig. S12a and b) exhibit similar peaks as PCN, indicative of their similar framework structure. In N 1s core-level spectra (Fig. S12c), PCN also exhibits typical four peaks at 398.6, 399.8, 401.1, and 404.3 eV, corresponding to C=N−C, N−H, N−C$_3$, and π excitation of the heptazine units [14], respectively, just like the melem [15]. The BM-PCN, BM-PCN/Co, BM-PCN/Co-c, and PCN/Co-c exhibit similar peaks as PCN (Fig. S12c and d), further manifesting their similar framework structure.
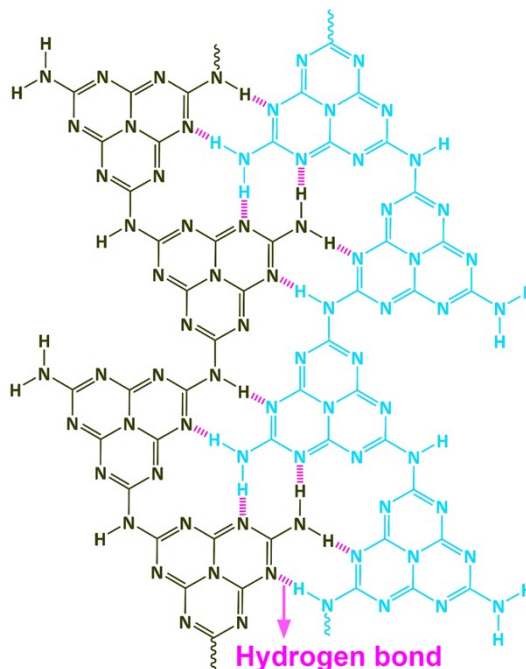
Fig. S13. Single-layer structure of PCN with intralayer hydrogen bonds revealed.
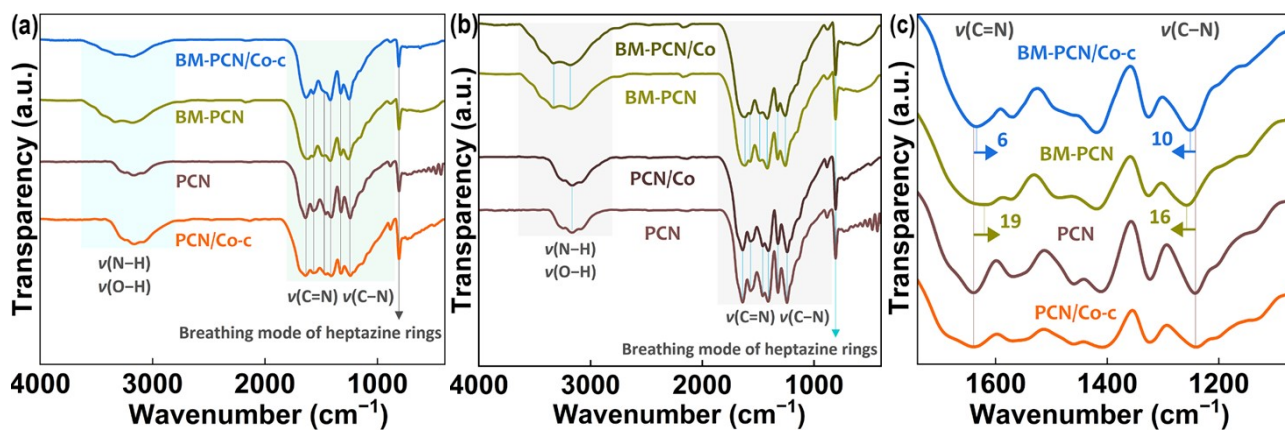
Fig. S14. FT-IR spectra of samples.

FT-IR spectra of the samples show similar absorption bands as reported melon-type PCN, i.e., those at ~3630–2800, ~1810–843, and 808 cm^{-1} assigned to O−H/N−H stretching vibrations, C=N/C−N stretching vibrations, and the out-of-plane bending mode of heptazine rings, respectively. [16, 17]
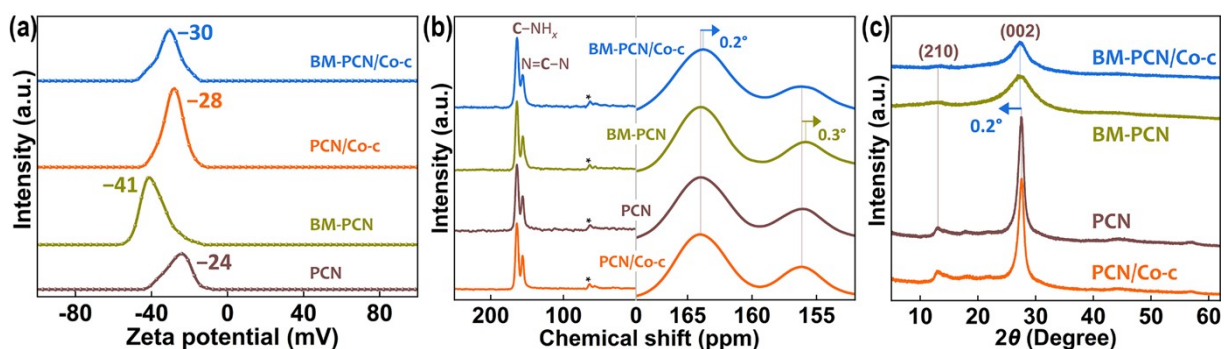
Fig. S15. (a) Zeta potentials of samples dispersed in water (0.2 g L^{-1}) with pH = 6.3±0.1; (b) solid-state ^{13}C MAS NMR spectra and (c) XRD patterns of the samples.
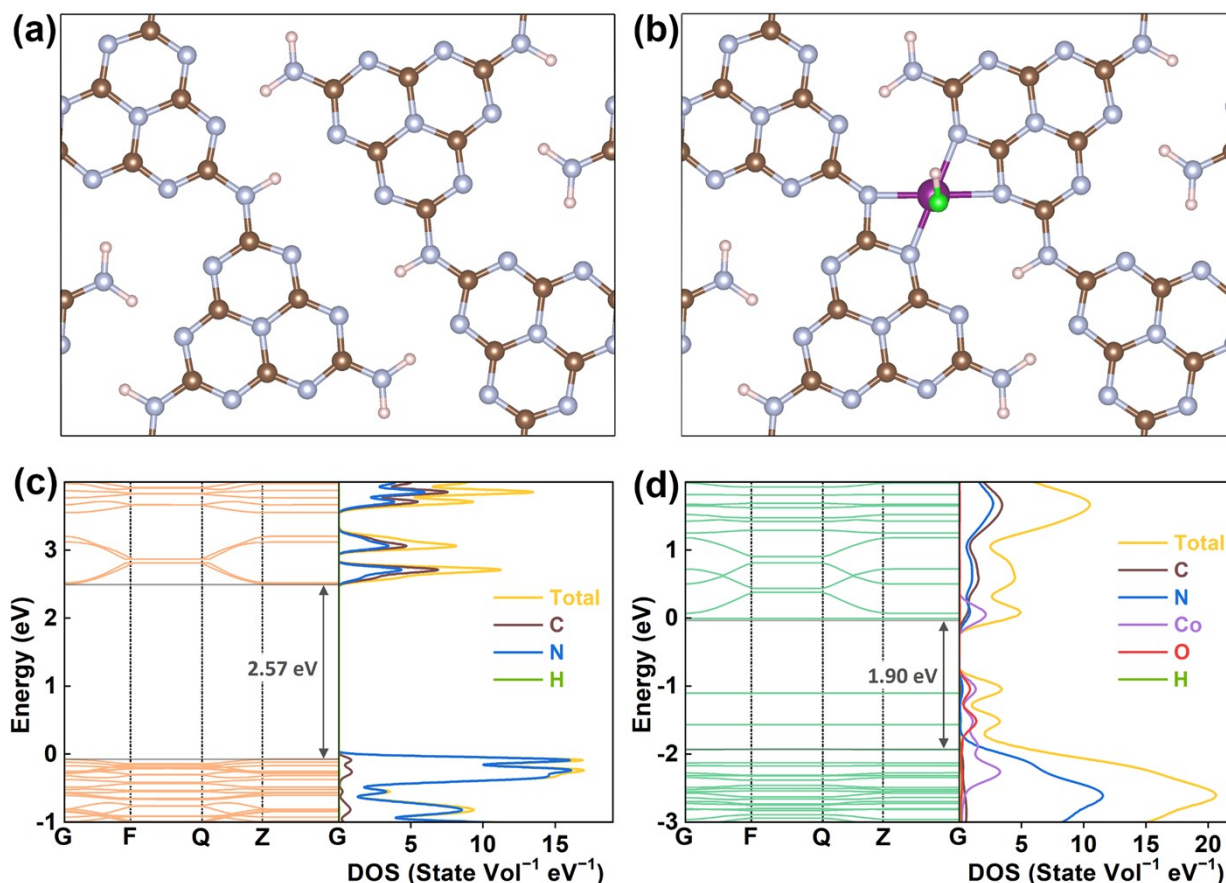
Fig. S16. Optimized structural models of (a) PCN and (b) BM-PCN/Co-c monolayers; and calculated energy bands and density of states (DOS) of (c) PCN and (d) BM-PCN/Co-c.
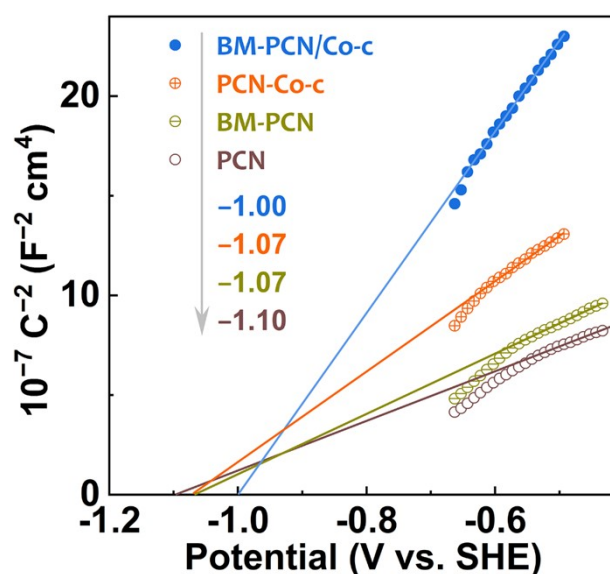
Fig. S17. Mott-Schottky plots of samples. Numbers in the figure are flat-band potentials.

For n-type semiconductors, E_{CB} are proximately regarded as their flat-band potentials (E_{fb}) which can be determined from Mott-Schottky plots, i.e., estimated as the intercept on the *x*-axis by extrapolating the Mott-Schottky curves, based on the equation, $C^{-2} = 2(e\varepsilon\varepsilon_0 N_D)^{-1}(E - E_{fb} - kTe^{-1})$ [18] where N_D, C, E, e, ε, ε_0, and k are charge carrier density, the capacitance of the space charge layer, the potential (vs. SHE), the electron charge, the dielectric constant, the vacuum permittivity, and the Boltzmann constant, respectively. As shown in the figure, positive slops of the extension lines manifest that PCN, BM-PCN, BM-PCN/Co-c, and PCN/Co-c are all n-type semiconductors, and their E_{fb} are determined as −1.10, −1.07, −1.00, and −1.07 V (vs. SHE), respectively.
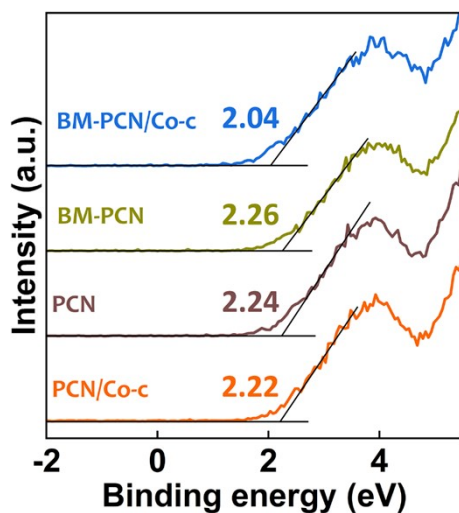
Fig. S18. VB-XPS spectra of samples.

VB-XPS spectroscopy was conducted to confirm the energy difference (E_d) between E_{VB} and the Fermi level (E_f) [19], and the E_d of PCN, BM-PCN, BM-PCN/Co-c, and PCN/Co-c was determined as 2.24, 2.26, 2.04, and 2.22 eV, respectively. Then, E_f ($E_f = E_{VB} - E_d$) of the samples was calculated to be –0.64, –0.52, –0.48, and –0.56 eV, respectively.
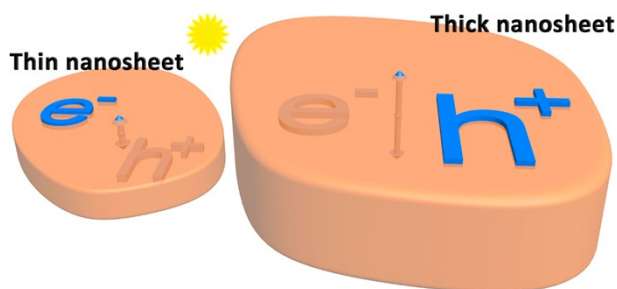
Fig. S19. Schematic illustration for photogenerated charge transfer distance from inside to surface of thin and thick nanosheets.
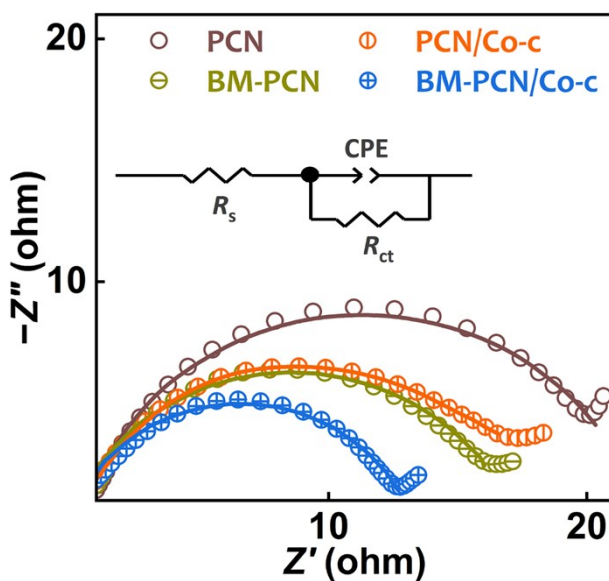
Fig. S20. EIS spectra of samples. The R_s, R_{ct}, and CPE represent the electrolyte resistance, the charge transfer resistance, and the double-layer capacitance, respectively
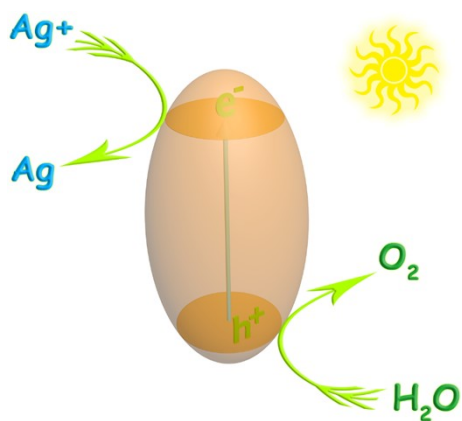
Fig. S21. Schematic illustration for photocatalytic OER using Ag^+ as the electron acceptor.
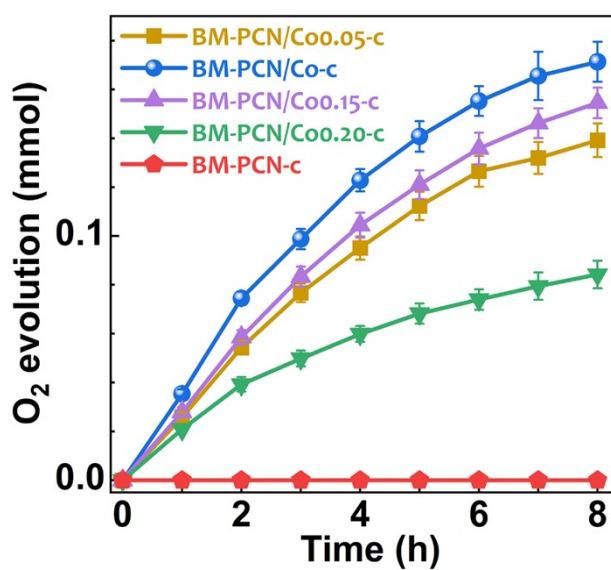
Fig. S22. The influence of Co concentration (x M) in initial suspensions on photocatalytic OER activity of BM-PCN/Co-c (x = 0.10) and BM-PCN/Cox-c.
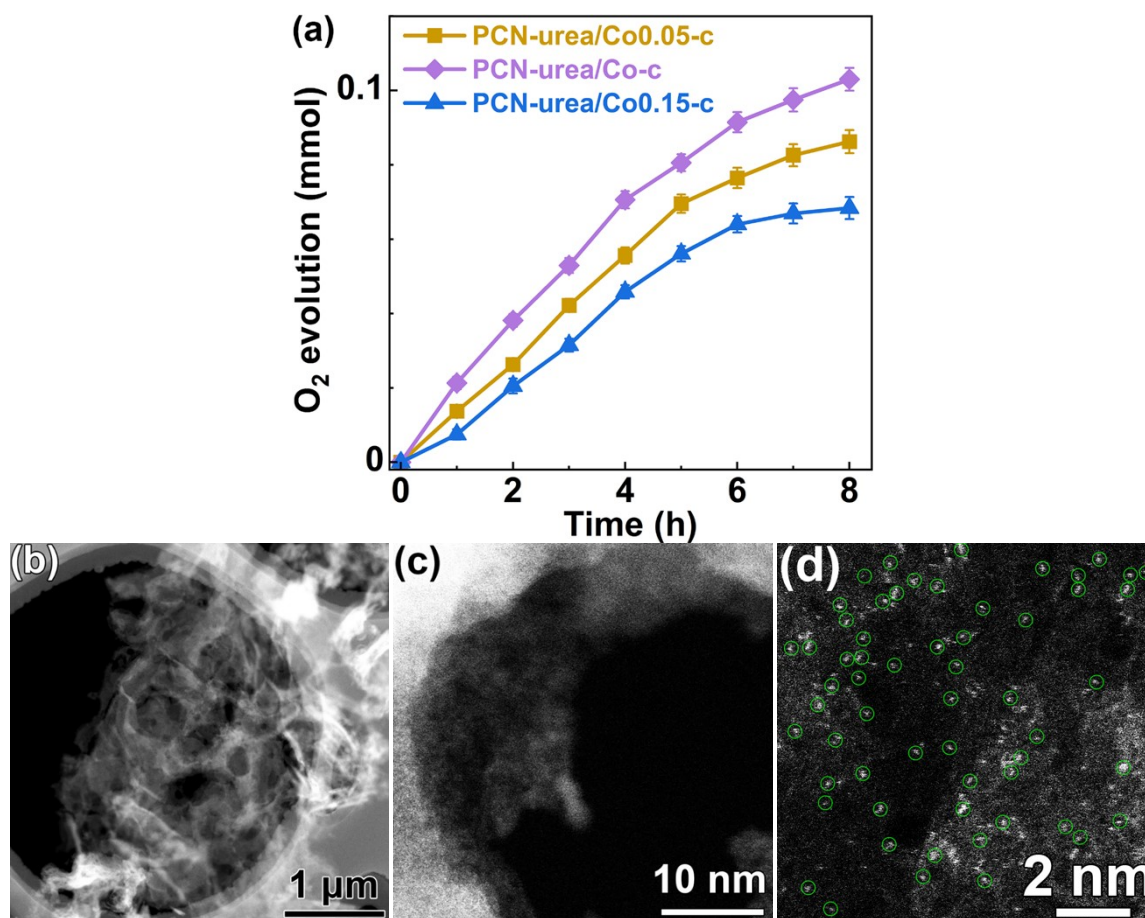
Fig. S23. (a) The influence of Co concentration (*x* M) in initial suspensions on photocatalytic OER activity of PCN-urea/Co-c (*x* = 0.10) and PCN-urea/Co*x*-c and (b–d) HAADF STEM images of PCN-urea/Co-c.
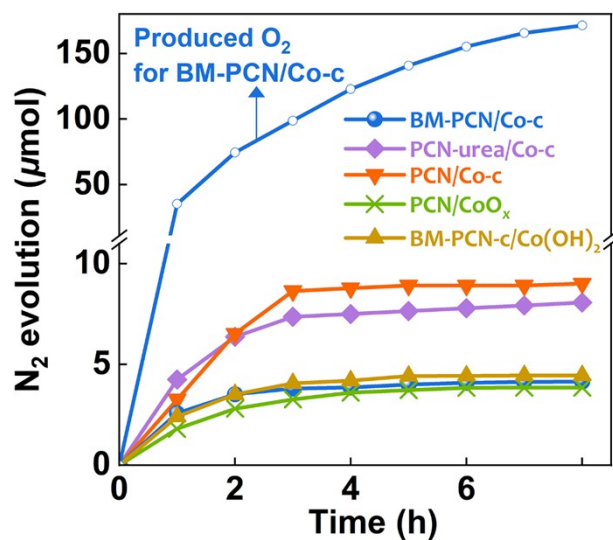
Fig. S24. Generated N₂ in photocatalytic OER processes under illumination of the Xe lamp for various samples. The OER curve of BM-PCN/Co-c is also shown in this figure.
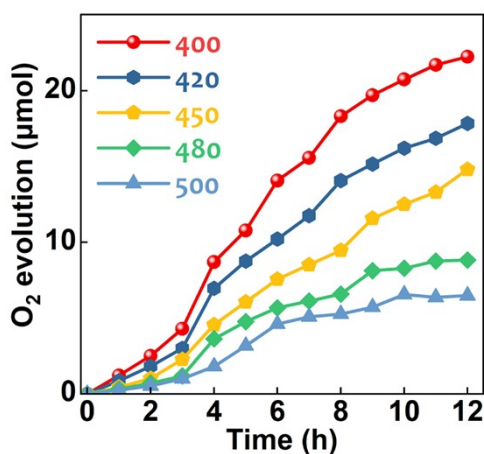
Fig. S25. Photocatalytic oxygen evolution on BM-PCN/Co-c under irradiation of monochromatic light with wavelengths of 400, 420, 450, 480, and 500 nm.
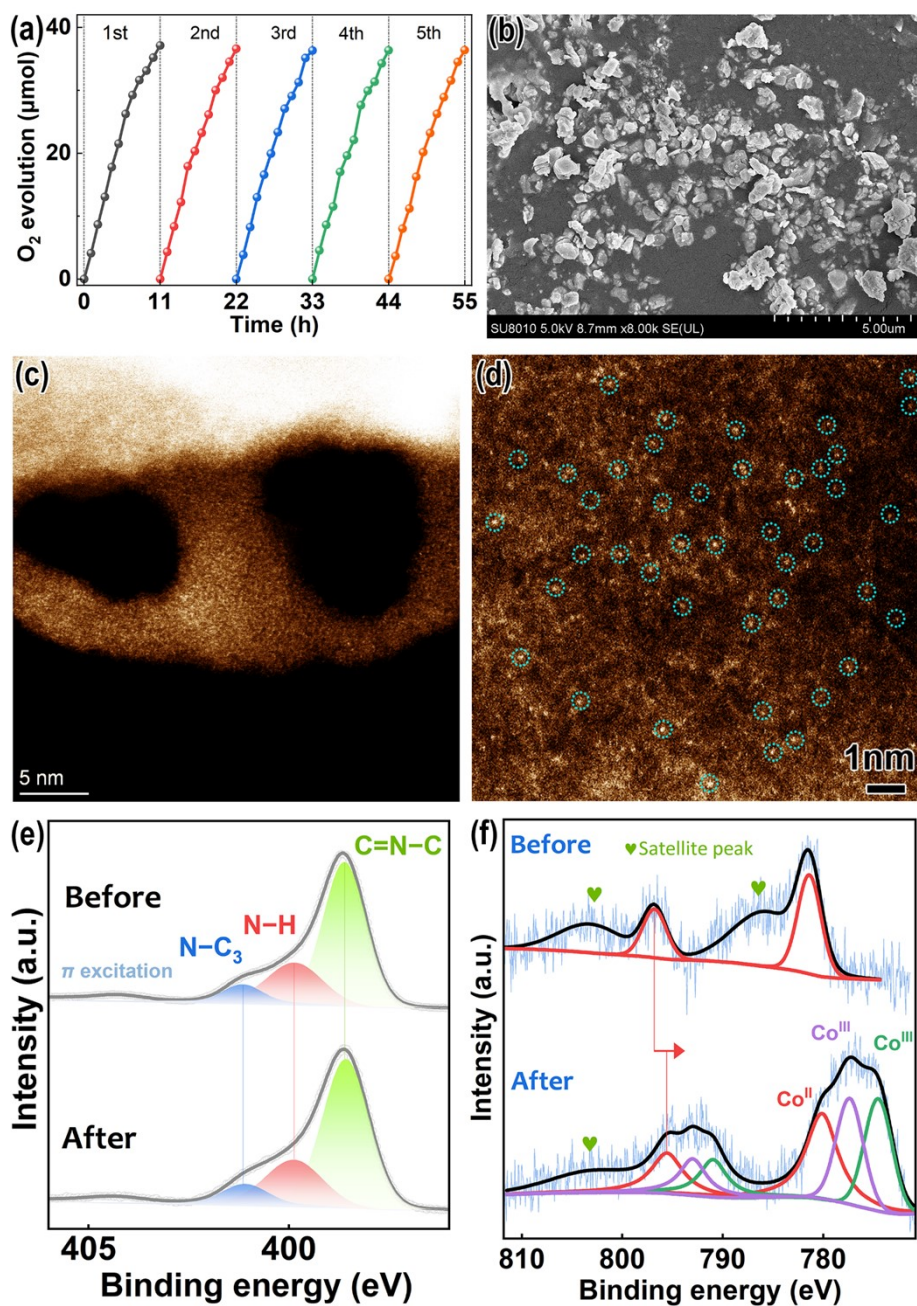
Fig. S26. (a) The cyclic experiment of photocatalytic oxygen evolution on BM-PCN/Co-c with 0.01 M KIO$_4$ as the electron acceptor; (b) SEM and (c and d) HAADF-STEM images of BM-PCN/Co-c after the cyclic experiment; and (e) N 1s and (f) Co 2p core-level XPS spectra of BM-PCN/Co-c before and after the cyclic experiment. Dotted circles in (d) mark the Co single atoms.

As shown in N 1s core-level XPS spectra, ~1.0 eV shift of Co^{II} peaks to low binding energy after the cyclic experiment likely arises from the ion adsorption on the Co^{II}–OH structure (e.g., IO$_4^-$Co^{II}–OH, and I$^-$Co^{II}–OH groups). New peaks at binding energy of 777.5 and 774.7 eV should correspond to Co 2p$_{3/2}$ of Co^{III} in different forms [20].

Table S1. Co K-edge EXAFS curve fitting parameters [a].

Samples	Path	R (Å)	N	σ^2 (Å^2)	ΔE_0 (eV)	R-factor
Co foil [b]	Co-Co	2.49	12 (Fixed)	0.0063	7.92	0.0019
BM-PCN/Co-c [c]	Co-N	2.06	5.6±0.4	0.0083	−1.98	0.0035
BM-PCN/Co-c [d]	Co-N	2.04	4 (Fixed)	0.0043	−1.26	0.0011
	Co-O	2.15	1 (Fixed)	0.0012	−0.65	

[a] N, coordination number; R, distance between absorber and backscatter atoms; σ^2, Debye-Waller factor to account for both thermal and structural disorders; ΔE_0, inner potential correction; R-factor indicates the goodness of the fit. S_0^2 was fixed to 0.78 as determined from Co foil fitting. The coordination number (N) of Co foil was fixed according to the crystal structure.
[b] Fitting range: 3.0 ≤ k (Å^{-1}) ≤ 12.4 and 1.0 ≤ R (Å) ≤ 3.0.
[c] Single-shell fitting with fitting range: 2.0 ≤ k (Å^{-1}) ≤ 12.5 and 1.0 ≤ R (Å) ≤ 2.0.
[d] Double-shell fitting with fitting range: 2.0 ≤ k (Å^{-1}) ≤ 12.5 and 1.0 ≤ R (Å) ≤ 2.0.

Table S2. Peak information from Co 2p and O 1s core-level XPS spectra of BM-PCN/Co-c.

Sample	Area (a.u.)		Sensitivity factor		Co/O(−Co) molar ratio
	Co	O(−Co)	Co	O	
BM-PCN/Co-c	5735	849	18.24	2.881	1.07

Table S3. Elemental analysis results of samples.

Sample	Content (wt%)			N/C molar ratio
	N	C	H	
PCN	61.91	34.77	2.00	1.53
BM-PCN	56.25	31.56	3.08	1.53
PCN/Co-c	60.22	33.96	2.28	1.52
BM-PCN/Co-c	58.01	32.78	2.38	1.52

Table S4. Photocatalytic O_2 evolution activity of reported PCN-based photocatalysts.

Sample	Light source | Electron scavenger	R_O [a]	λ_A (nm)	AQY [b] (%)	Ref.
CN of S-mediated synthesis	300-W Xe lamp ($\lambda > 300$ nm) | AgNO$_3$ (0.01 M)	20.1	\	\	[21]
Fish scale-like PCN/Ag$_3$PO$_4$	White light LED | AgNO$_3$ (10 g L^{-1})	6.8	\	\	[22]
Co$_3$O$_4$/helical PCN	300-W Xe lamp ($\lambda > 300$ nm) | AgNO$_3$ (0.01 M)	3.6	\	\	[23]
Br modified PCN	300-W Xe lamp | AgNO$_3$ (0.01 M)	23.0	\	\	[24]
	300-W Xe lamp ($\lambda \geq 420$ nm) | AgNO$_3$ (0.01 M)	4.0			
Co(OH)$_2$-Co$_3$O$_4$/PCN	300-W Xe lamp ($\lambda > 420$ nm) | Na$_2$SO$_4$, Na$_2$S$_2$O$_8$, [Ru(bpy)$_3$]Cl$_2$	3.7	\	\	[25]
NiCoP@NiCo-Pi/PCN	300-W Xe lamp ($\lambda > 300$ nm) | AgNO$_3$ (0.02 M)	15.6	380	0.6	[26]
CoMn$_2$O$_4$/PCN	300-W Xe lamp ($\lambda > 300$ nm) | AgNO$_3$ (0.01 M)	18.3	380	1.0	[27]
B doped deficient PCN	300-W Xe lamp ($\lambda > 300$ nm) | AgNO$_3$ (0.01 M)	28.1	380	3.7	[28]
	300-W Xe lamp ($\lambda \geq 420$ nm) | AgNO$_3$ (0.01 M)	8.0			
	300-W Xe lamp ($\lambda \geq 450$ nm) | AgNO$_3$ (0.01 M)	2.4			
mpg-PCN$_x$/CoO/CoPi	Visible light (100 mW cm^{-2}, $\lambda > 400$nm) | Na$_2$S$_2$O$_8$ (0.1 M)	30.4	\	\	[29]
Ni-Co LDH/PCN	300-W Xe lamp ($\lambda > 300$ nm) | AgNO$_3$ (0.01 M)	26.7	\	\	[30]
CoSe$_2$/PCN	300-W Xe lamp ($\lambda > 300$ nm) | AgNO$_3$ (0.01 M)	33.5	\	\	[31]
RuO$_2$/PCN	300-W Xe lamp ($\lambda > 300$ nm) | AgNO$_3$ (0.01 M)	11.4	\	\	[32]
	300-W Xe lamp ($\lambda > 420$ nm) | AgNO$_3$ (0.01 M)	1.2			
Ag$_3$PO$_4$/ PCN nanorods	LED light | AgNO$_3$ (10 g L^{-1})	11.0	\	\	[33]
Co(OH)$_2$/PCN	300-W Xe lamp ($\lambda > 300$ nm) | AgNO$_3$ (0.01 M)	27.4	\	\	[2]
	300-W Xe lamp ($\lambda > 450$ nm) | AgNO$_3$ (0.01 M)	1.4			
S-doped PCN/BiVO$_4$	300-W Xe lamp ($\lambda > 420$ nm) | AgNO$_3$ (0.05 M)	15.0	\	\	[34]
Ag$_3$PO$_4$/PCN	LED white-light module | AgNO$_3$ (10 g L^{-1})	6.4	\	\	[35]
Co$_3$O$_4$/PCN	300-W Xe lamp ($\lambda > 420$ nm) | AgNO$_3$ (0.01 M)	25.1	420	1.1	[36]
Co doped PCN	300-W Xe lamp ($\lambda > 300$ nm) | AgNO$_3$ (0.01 M)	13.0	\	\	[37]
Nitrogen defective PCN	300-W Xe lamp | AgNO$_3$ (0.01 M)	8	\	\	[38]
CoN/PCN	300-W Xe lamp ($\lambda > 420$ nm) | AgNO$_3$ (0.025 M)	30.4	\	\	[39]
Cobalt-oxo cubane/PCN	300-W Xe lamp ($\lambda > 420$ nm) | Na$_2$S$_2$O$_8$ (0.05 M)	6.9	\	\	[40]
CoAl$_2$O$_4$/PCN	300-W Xe lamp ($\lambda \geq 400$ nm) | AgNO$_3$ (0.01 M)	2.7	\	\	[41]
Oxygen-rich Co$_3$O$_4$ with the (222) facet/PCN nanofiber	300-W Xe lamp ($\lambda > 420$ nm) | AgNO$_3$ (0.01 M)	24.9	\	\	[42]
Ag$_3$PO$_4$/KOH-treated PCN	LED light | AgNO$_3$ (10 g L^{-1})	9.3	\	\	[43]
LaOCl/PCN	300-W Xe lamp ($\lambda > 300$ nm) | AgNO$_3$ (0.01 M)	10.7	\	\	[44]
	300-W Xe lamp ($\lambda > 400$ nm) | AgNO$_3$ (0.01 M)	3.8			
BM-PCN/Co-c			400	4.7	
	200-W Xe lamp | AgNO$_3$ (0.1 M)	44.3	420	2.1	This
	200-W Xe lamp ($\lambda \geq 420$ nm) | AgNO$_3$ (0.1 M)	37.3	450	1.1	work
			500	0.5	

[a] Photocatalytic O_2 evolution rate (μmol h^{-1}); [b] Apparent quantum yield at the wavelength of λ_A

Reference

1   G. Zhang, Z. A. Lan, L. Lin, S. Lin and X. Wang, *Chem. Sci.*, 2016, **7**, 3062.

2   G. Zhang, S. Zang and X. Wang, *ACS Catal.*, 2015, **5**, 941.

3   H. Wang, S. Jiang, S. Chen, X. Zhang, W. Shao, X. Sun, Z. Zhao, Q. Zhang, Y. Luo and Y. Xie, *Chem. Sci.*, 2017, **8**, 4087.

4   N. K. Veldurthi, N. K. Eswar, S. A. Singh and G. Madras, *Catal. Sci. Technol.*, 2018, **8**, 1083.

5   G. Kresse and D. Joubert, *Phys. Rev. B*, 1999, **59**, 1758.

6   G. Kresse and J. Furthmüller, *Comp. Mater. Sci.*, 1996, **6**, 15.

7   G. Kresse and J. Furthmüller, *Phys. Rev. B*, 1996, **54**, 11169.

8   J. P. Perdew, K. Burke and M. Ernzerhof, *Phys. Rev. Lett.*, 1996, **77**, 3865.

9   S. Grimme, J. Antony, S. Ehrlich and H. Krieg, *J. Chem. Phys.*, 2010, **132**, 154104.

10   F. Fina, S. K. Callear, G. M. Carins and J. T. S. Irvine, *Chem. Mater.*, 2015, **27**, 2612.

11   D. L. Yu, J. L. He, Z. Y. Liu, B. Xu, D. C. Li and Y. J. Tian, *J. Mater. Sci.*, 2007, **43**, 689.

12   C. Chang, Y. Fu, M. Hu, C. Wang, G. Shan and L. Zhu, *Appl. Catal. B*, 2013, **142-143**, 553.

13   A. P. Dementjev, A. de Graaf, M. C. M. van de Sanden, K. I. Maslakov, A. V. Naumkin and A. A. Serov, *Diamond Relat. Mater.*, 2000, **9**, 1904.

14   H. Katsumata, K. Sakakibara, I. Tateishi, M. Furukawa and S. Kaneco, *Catal. Today*, 2019, 47.

15   C. M. Zhu, A. Gao, Y. Wang and Y. Liu, *Chem. Commun.*, 2014, **50**, 13889.

16   Y. Xie, Y. Li, Z. Huang, J. Zhang, X. Jia, X.-S. Wang and J. Ye, *Appl. Catal. B*, 2020, **265**, 118581.

17   Y. Li, S. Ouyang, H. Xu, X. Wang, Y. Bi, Y. Zhang and J. Ye, *J. Am. Chem. Soc.*, 2016, **138**, 13289.

18   G. Liu, G. Zhao, W. Zhou, Y. Liu, H. Pang, H. Zhang, D. Hao, X. Meng, P. Li, T. Kako and J. Ye, *Adv. Funct. Mater.*, 2016, **26**, 6822.

19   R. Schafranek, S. Payan, M. Maglione and A. Klein, *Phys. Rev. B*, 2008, **77**, 195310.

20   W. Xu, Z. Xie, Z. Wang, G. Dietrich and Y. Wang, *J. Mater. Chem. A*, 2016, **4**, 19011.

21   J. Zhang, J. Sun, K. Maeda, K. Domen, P. Liu, M. Antonietti, X. Fu and X. Wang, *Energy Environ. Sci.*, 2011, **4**, 675.

22   X. Yang, L. Tian, X. Zhao, H. Tang, Q. Liu and G. Li, *Appl. Catal. B*, 2019, **244**, 240.

23   Y. Zheng, L. Lin, X. Ye, F. Guo and X. Wang, *Angew. Chem. Int. Ed.*, 2014, **53**, 11926.

24   Z.-A. Lan, G. Zhang and X. Wang, *Appl. Catal. B*, 2016, **192**, 116.

25   H. Zhang, W. Tian, X. Guo, L. Zhou, H. Sun, M. O. Tadé and S. Wang, *ACS Appl. Mater. Interfaces*, 2016, **8**, 35203.

26   Z. Qin, Y. Chen, Z. Huang, J. Su and L. Guo, *J. Mater. Chem. A*, 2017, **5**, 19025.

27   L. Zhang, C. Yang, Z. Xie and X. Wang, *Appl. Catal. B*, 2018, **224**, 886.

28   D. Zhao, C. L. Dong, B. Wang, C. Chen, Y. C. Huang, Z. Diao, S. Li, L. Guo and S. Shen, *Adv. Mater.*, 2019, **31**, e1903545.

29   R.-L. Lee, P. D. Tran, S. S. Pramana, S. Y. Chiam, Y. Ren, S. Meng, L. H. Wong and J. Barber, *Catal. Sci. Technol.*, 2013, **3**, 1694.

30   M. Zhang, Z. Luo, M. Zhou, G. Zhang, K. A. Alamry, L. A. Taib, A. M. Asiri and X. Wang, *Appl. Catal. B*, 2017, **210**, 454.

31   G. Zhang, S. Zang, Z.-A. Lan, C. Huang, G. Li and X. Wang, *J. Mater. Chem. A*, 2015, **3**, 17946.

32   K. Maeda, X. Wang, Y. Nishihara, D. Lu, M. Antonietti and K. Domen, *J. Phys. Chem. C*, 2009, **113**, 4940.

33   L. Tian, X. Xian, X. Cui, H. Tang and X. Yang, *Appl. Surf. Sci.*, 2018, **430**, 301.

34   H. J. Kong, D. H. Won, J. Kim and S. I. Woo, *Chem. Mater.*, 2016, **28**, 1318.

35   X. Yang, H. Tang, J. Xu, M. Antonietti and M. Shalom, *ChemSusChem*, 2015, **8**, 1350.

36   J. Zhang, M. Grzelczak, Y. Hou, K. Maeda, K. Domen, X. Fu, M. Antonietti and X. Wang, *Chem. Sci.*, 2012, **3**, 443.

37   G. Zhang, C. Huang and X. Wang, *Small*, 2015, **11**, 1215.

38   P. Yang, L. Wang, H. Zhuzhang, R. Wang, M.-M. Titirici and X. Wang, *Appl. Catal. B*, 2019, **256**, 117794.

39   J. Zhang, G. Zhang and J. Zhang, *Appl. Surf. Sci.*, 2019, **475**, 256.

40   W. Zhen, X. Yuan, X. Shi and C. Xue, *Chem. Asian J.*, 2020, **15**, 2480.

41   T. Kanazawa, K. Kato, R. Yamaguchi, T. Uchiyama, D. Lu, S. Nozawa, A. Yamakata, Y. Uchimoto and K. Maeda, *ACS Catal.*, 2020, **10**, 4960.

42   Y. Zeng, H. Li, Y. Xia, L. Wang, K. Yin, Y. Wei, X. Liu and S. Luo, *ACS Appl. Mater. Interfaces*, 2020, **12**, 44608.

43   C. Zhao, L. Tian, Z. Zou, Z. Chen, H. Tang, Q. Liu, Z. Lin and X. Yang, *Appl. Catal. B*, 2020, **268**, 118445.

44   Y. Lin, W. Su, X. Wang, X. Fu and X. Wang, *Angew. Chem. Int. Ed.*, 2020, **59**, 20919.